

## Estimating relativistic electron pitch angle scattering rates using properties of the electromagnetic ion cyclotron wave spectrum

T. M. Loto'aniu,<sup>1,2</sup> R. M. Thorne,<sup>1</sup> B. J. Fraser,<sup>3</sup> and D. Summers<sup>4,5</sup>

Received 30 September 2005; revised 12 January 2006; accepted 23 January 2006; published 29 April 2006.

[1] An EMIC wave event observed by the CRRES spacecraft during an active period on 11 August 1991 was studied in order to estimate electron minimum interaction kinetic energy  $E_{\min}$  and using quasilinear theory, to calculate the resonant scattering rate  $D_{\alpha\alpha}$ . The wave packet semibandwidth  $\delta\omega/2\pi$  full-width half maximum ranged from 0.06 Hz to 0.27 Hz. Resonant scattering was assumed to occur over the frequency interval  $\omega_m - \delta\omega$  to  $\omega_m + \delta\omega$ . Assuming typical stormtime ion concentrations, the use of realistic wave spectral properties when compared to only using the central wave frequency  $\omega_m$  results in 3 to 4 times as many wave packets that are able to interact with relativistic electrons below  $\sim 2$  MeV. Values of  $D_{\alpha\alpha}$  associated with two of the wave packets, where  $E_{\min}$  falls to within the 1–2 MeV energy range, were comparable to the limit of strong diffusion suggesting enhanced electron precipitation. CRRES observed an  $\sim 1$  order of magnitude decrease in the 1–2 MeV electron flux levels during the EMIC wave interval. It is suggested that this flux decrease was due to EMIC waves pitch angle scattering the relativistic electrons. The EMIC waves were observed near the start of the main phase of a geomagnetic storm. This study strengthens the suggestion that relativistic electron scattering by EMIC waves can compete with the *Dst* effect as a mechanism of decreasing relativistic electron fluxes from the outer zone during magnetic storms.

**Citation:** Loto'aniu, T. M., R. M. Thorne, B. J. Fraser, and D. Summers (2006), Estimating relativistic electron pitch angle scattering rates using properties of the electromagnetic ion cyclotron wave spectrum, *J. Geophys. Res.*, *111*, A04220, doi:10.1029/2005JA011452.

### 1. Introduction

[2] Relativistic electron ( $>1$  MeV) flux levels in the Earth's radiation belts are extremely variable, particularly during geomagnetic storms [e.g., *Blake et al.*, 1992; *Baker et al.*, 1994; *Li et al.*, 1997]. However, the mechanisms responsible for this flux variation are not well understood [e.g., *Fung*, 2004]. Although much work has been directed at trying to explain the acceleration mechanisms [*Summers et al.*, 1998; *Rostoker et al.*, 1998; *Elkington et al.*, 1999; *Mathie and Mann*, 2000, 2001; *O'Brien et al.*, 2003; *Friedel et al.*, 2002; *Elkington et al.*, 2003] loss processes are just as important since the competition between loss and acceleration determine the overall flux levels [e.g., *Reeves et al.*, 2003; *Meredith et al.*, 2003; *Summers et al.*, 2004]. It

has been shown that the time taken for electron losses is comparable to the acceleration timescale [e.g., *Summers and Thorne*, 2003].

[3] Typically, relativistic electron flux levels fall by up to two or three orders of magnitude during the main phase of storms [e.g., *Meredith et al.*, 2002]. During the recovery phase the flux usually increases to the pre-storm levels or higher. However, 25% of storms lead to a net decrease in flux levels [*Reeves et al.*, 2003]. The large flux decreases during the main phase is usually attributed to the *Dst* effect, where the relativistic electrons adiabatically respond to the decrease in the geomagnetic field strength caused by ring current enhancement [*Kim and Chan*, 1997; *Kim et al.*, 2002]. However, particle losses to the atmosphere and magnetopause would also result in flux decreases.

[4] Recent theoretical calculations by *Summers and Thorne* [2003] suggest that pitch angle scattering can compete with the *Dst* effect as a mechanism for depleting relativistic electrons from the outer zone during the initial and main phases of a magnetic storm. The flux decreases during the initial and main phase of a storm is likely to be caused by a combination of the *Dst* effect, rapid pitch angle scattering loss to the atmosphere, and drift loss to the magnetopause [e.g., *Thorne et al.*, 2005]. The contribution from each of these mechanisms remains to be quantified. Identifying the likely contributions from each of these mechanisms is important and essential to further our under-

<sup>1</sup>Department of Atmospheric Sciences, University of California, Los Angeles, Los Angeles, California, USA.

<sup>2</sup>Now at Department of Physics, University of Alberta, Edmonton, Alberta, Canada.

<sup>3</sup>Cooperative Research Centre for Satellite Systems, School of Mathematical and Physical Sciences, University of Newcastle, Newcastle, New South Wales, Australia.

<sup>4</sup>Department of Mathematics and Statistics, Memorial University of Newfoundland, St. John's, Newfoundland, Canada.

<sup>5</sup>Also at School of Physics, University of KwaZulu-Natal, Durban, South Africa.

standing of the behavior of relativistic electrons during storms.

[5] Electromagnetic ion cyclotron (EMIC) waves propagating in the magnetosphere are thought to interact with relativistic electrons through cyclotron resonance and cause pitch angle scattering of the electrons [e.g., *Thorne and Kennel, 1971; Lyons and Thorne, 1972; Thorne and Andreoli, 1980; Horne and Thorne, 1998; Summers et al., 1998; Summers and Thorne, 2003*]. This wave-particle gyroresonant interaction is thought to cause significant electron losses to the atmosphere over many drift orbits. However, direct evidence of relativistic electron precipitation due to scattering by EMIC waves is limited because of the difficulty of measuring the precipitating electrons in the low altitude regions and the waves at high altitudes simultaneously. There have been measurements using balloons of X-ray bursts in the duskside which were consistent with bremsstrahlung emission from relativistic ( $\geq 1.0$  MeV) precipitating electrons due to pitch angle scattering by gyroresonance with EMIC waves [*Foat et al., 1998; Lorentzen et al., 2000; Millan, 2002*]. The EMIC waves occur most frequently and intensely during geomagnetic storms [*Bräysy et al., 1998; Erlandson and Ukhorskiy, 2001*] and are generated and amplified near the equatorial region of the Earth's magnetosphere [e.g., *Fraser et al., 1996; Loto'aniu et al., 2005*] by energetic ring current ions (10–100 keV) through ion cyclotron instabilities. They are usually left-hand (LH) polarized (L-mode) with respect to the background magnetic field and when detected on the ground are seen as 1–10 nT perturbations on the background field with frequencies in the 0.1–5.0 Hz, or Pc1 ULF wave range. They are observed most frequently in the afternoon and duskside and over  $L$ -value ranges  $L > 3$  [e.g., *Fraser and Nguyen, 2001; Loto'aniu et al., 2005*].

[6] A recent extensive statistical study by *Meredith et al. [2003]* of the minimum resonant energy  $E_{\min}$  required by electrons to interact with EMIC waves in the inner magnetosphere found that  $E_{\min}$  was generally above 2 MeV. However, they also found that  $E_{\min}$  can fall below 2 MeV in localized regions of high plasma density and/or low magnetic field for wave frequencies just below the H<sup>+</sup> cyclotron ( $f_H$ ) or He<sup>+</sup> cyclotron ( $f_{He}$ ) frequencies. These lower energy scattering events were mainly associated with L-mode EMIC waves. Meredith et al. assumed the EMIC wave frequency to be the central wave frequency,  $\omega_m$ . However, in reality each wave packet covers a range of frequencies and can therefore interact with electrons over a range of energies.

[7] In this paper, an EMIC wave event observed by the CRRES spacecraft on 11 August 1991 is studied in order to calculate the electron minimum interaction energies and resonant scattering rates using realistic EMIC wave spectral properties. Section 2 briefly describes the CRRES instrumentation of importance to the study. In sections 3 and 4, derivations by *Summers and Thorne [2003]* of the resonant energy and pitch angle diffusion coefficient are summarized. Presented in section 5 are the results, while section 6 discusses these results and section 7 briefly summarizes the important conclusions.

## 2. Instrumentation

[8] The CRRES spacecraft operated for about 15 months during 1990–1991 and observed the inner magnetosphere

over  $L = 3–8$  and up to  $\sim 30^\circ |MLat|$ . The CRRES orbit drift allowed local time coverage only over 1400–0800 MLT, unless the spacecraft was off the equator [*Johnson and Ball, 1992*]. The AGFL fluxgate magnetometer provided three component vector magnetic field data from DC-8 Hz Nyquist [*Singer et al., 1992*]. The University of Iowa/AFGL Plasma Waves Experiment (PWE) was used to estimate cold electron plasma densities  $N_e$  through observations of the upper hybrid resonance frequency ( $f_{UHR}$ ) [*Anderson et al., 1992*]. The relativistic electron (1–2 MeV) data were measured by the magnetic electron spectrometer, also known as the MEA (Medium Electrons A), which had a raw resolution of  $\sim 0.5$  s [*Johnson and Ball, 1992*]. For this study, the MEA data were 1-min averaged.

## 3. Electron Resonance and Minimum Energy

[9] The relativistic Doppler shifted resonance condition for interaction between electrons of cyclotron frequency  $\Omega_e$  and parallel L-mode propagating EMIC waves of frequency  $\omega$  and wave number  $k_{\parallel}$  is

$$\omega - k_{\parallel}v_{\parallel} = -|\Omega_e|/\gamma, \quad (1)$$

where  $\gamma = (1 - v^2/c^2)^{-1/2}$  and  $v^2 = v_{\perp}^2 + v_{\parallel}^2$  [e.g., *Summers and Thorne, 2003*]. The dispersion relation for (L-mode) EMIC waves propagating parallel to the background magnetic field in a cold uniform H<sup>+</sup>-He<sup>+</sup>-O<sup>+</sup> ion plasma is

$$\frac{1}{u^2} = 1 - \frac{1}{\zeta \epsilon X} \left( \frac{1}{1 + \epsilon X} + \frac{\eta_H}{X - 1} + \frac{\eta_{He}}{4X - 1} + \frac{\eta_O}{16X - 1} \right), \quad (2)$$

where  $X = \omega/\Omega_H$  defines the local wave frequency  $\omega$  normalized to the local H<sup>+</sup> cyclotron frequency  $\Omega_H$ , while  $u = \omega/(kc)$  is the normalized wave phase speed and  $\epsilon = m_e/m_p$  the ratio of the electron mass  $m_e$  to proton mass  $m_p$ . Also,

$$\eta_H + \eta_{He} + \eta_O = 1 \quad (3)$$

defines the heavy ion ratios, while  $\zeta$  is given by

$$\zeta = \frac{\Omega_e^2}{\omega_{pe}^2} = \frac{B_o^2}{4\pi N_e} \cdot \frac{1}{m_e c^2}, \quad (4)$$

where  $\Omega_e$  is the electron cyclotron and  $\omega_{pe}$  the electron plasma frequencies. Here  $B_o$  is the background field strength and  $N_e$  the electron number density, which when assuming charge neutrality is equal to the plasma number density.

[10] The minimum kinetic energy  $E_{\min}$  required by an electron for cyclotron resonance interaction occurs when  $v_{\perp} = 0$ . This is when  $v_{\parallel}$  reaches a maximum  $(v_{\parallel})_m$  and the minimum energy, in units of  $m_e c^2$  is

$$E_{\min} = \left[ 1 - (v_{\parallel})_m^2/c^2 \right]^{-1/2} - 1, \quad (5)$$

where

$$\frac{(v_{\parallel})_m}{c} = \frac{u \left[ \epsilon^2 X^2 + (\epsilon^2 X^2 + u^2(1 - \epsilon^2 X^2))^{1/2} \right]}{\epsilon^2 X^2 + u^2}. \quad (6)$$

As previously mentioned, observations of EMIC waves in the magnetosphere show wave power covering a range of frequencies [e.g., *Loto'aniu et al.*, 2005]. Assuming this frequency bandwidth covers the range  $\omega_1 \leq \omega \leq \omega_2$ , or alternatively in terms of wave numbers the range  $k_1 \leq k \leq k_2$ , the electrons resonant with the waves have kinetic energy  $E$  and pitch angle  $\alpha$  restricted by the condition

$$\frac{\Omega_e^2}{c^2 k_2^2} \leq E(E+2) \cos^2 \alpha \leq \frac{\Omega_e^2}{c^2 k_1^2}. \quad (7)$$

In deriving equation (7) the  $\omega$ -term in equation (1) was neglected, which is justified since in the magnetosphere  $\omega/\Omega_e \ll 1$  [see *Summers and Thorne*, 2003]. Equation (7) shows that a range of  $E$  and  $\alpha$  will interact with an EMIC wave packet.

#### 4. Pitch Angle Diffusion

[11] The scattering of relativistic electrons by small-amplitude parallel propagating electromagnetic waves can be treated by quasilinear diffusion theory [e.g., *Steinacker and Miller*, 1992]. Using quasilinear theory and assuming a Gaussian wave power spectrum, *Summers and Thorne* [2003] derived a simple functional form for the pitch angle diffusion coefficient  $D_{\alpha\alpha}$  given by

$$D_{\alpha\alpha} = \frac{|\Omega_e|}{(E+1)} \cdot \frac{2R}{v\delta X} \cdot \left( \frac{\zeta\epsilon X^2 - Y}{2\zeta\epsilon X - Z} \right) e^{-[(X-X_m)/\delta X]^2}, \quad (8)$$

where

$$Y = X \left\{ \frac{1}{1+\epsilon X} + \frac{\eta_H}{X-1} + \frac{\eta_{He}}{4X-1} + \frac{\eta_O}{16X-1} \right\} \quad (9)$$

$$Z = \frac{1}{(1+\epsilon X)^2} + \frac{\eta_H}{(X-1)^2} + \frac{\eta_{He}}{(4X-1)^2} + \frac{\eta_O}{(16X-1)^2}, \quad (10)$$

and

$$R = \frac{\delta B^2}{B_o^2} \quad (11)$$

is the ratio of the magnetic field wave power  $\delta B^2$ , integrated over the signal bandwidth, to the background magnetic power  $B_o^2$  and  $v = \sqrt{\pi} \operatorname{erf}(1) \approx 1.49$ . The exponential in equation (8) is the assumed Gaussian shaped spectrum with

$$X_m = \frac{\omega_m}{\Omega_H}, \quad \delta X = \frac{\delta\omega}{\Omega_H}, \quad \text{and} \quad X = \frac{\omega}{\Omega_H}, \quad (12)$$

where  $\omega_m$  is the central wave frequency and  $\delta\omega$  the signal semi-bandwidth or standard deviation. The pitch angle  $\alpha$  can be written as

$$\cos \alpha = \left[ E(E+2) \left( \epsilon^2 X^2 - \frac{\epsilon}{\zeta} Y \right) \right]^{-1/2}, \quad (13)$$

where  $E$  and  $\alpha$  are restricted by equation (7). The following section presents the results along with a description of the

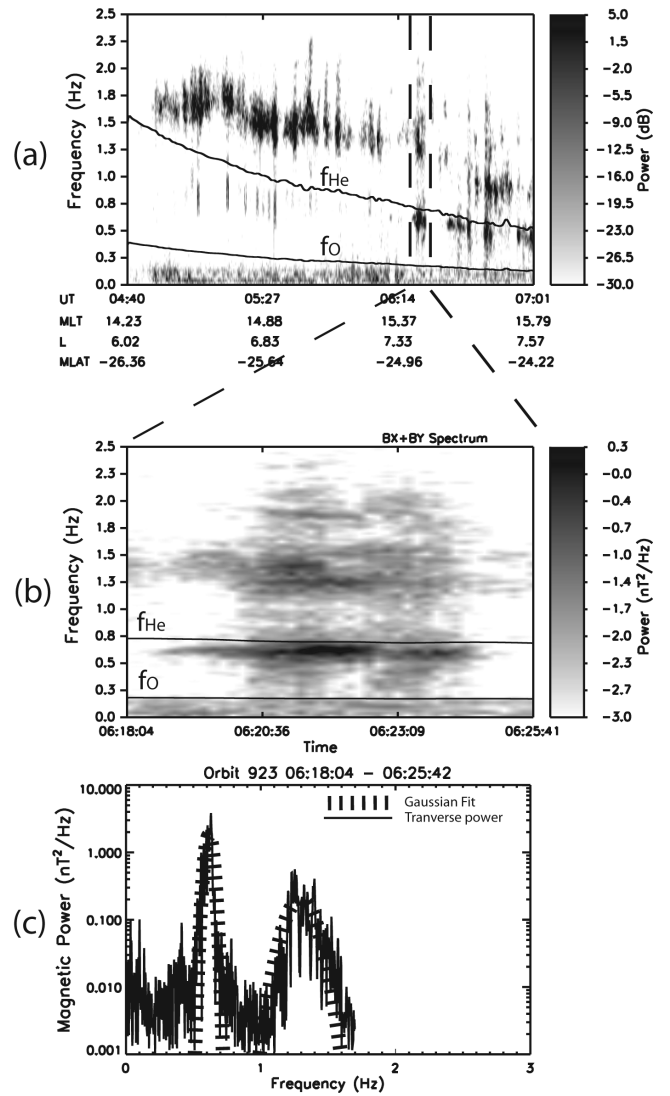


**Figure 1.** (a) Magnetic crosspower spectrogram for an EMIC wave event from CRRES orbit 923 on 11 August 1991. (b) Expanded view of the interval 0618–0625 UT magnetic transverse power. (c) The static magnetic transverse power of the interval 0618–0625 UT, with the dashed line representing the Gaussian fit to the two wave packets.

methods used to estimate the parameters used in the  $E_{\min}$  and  $D_{\alpha\alpha}$  calculations.

## 5. Results

### 5.1. Wave Spectral Power and Gaussian Fits

[12] The long duration event observed by CRRES during orbit 923 on 11 August 1991 is shown in Figure 1a. The event was observed by CRRES in the interval  $\sim 0500$ – $0700$  UT (14.4–15.8 MLT) or after local noon and over a magnetic latitude range of  $-26^\circ$  to  $-24^\circ$  and  $L = 6.3$ – $7.6$ . CRRES was moving outbound in the plasmatrough but close to apogee. The  $Dst$  and  $k_p$  values for 11 August are shown in Figure 2 with two vertical lines indicating the event interval ( $\sim 0500$ – $0700$  UT). The EMIC wave event occurred during the initial phase of a geomagnetic storm

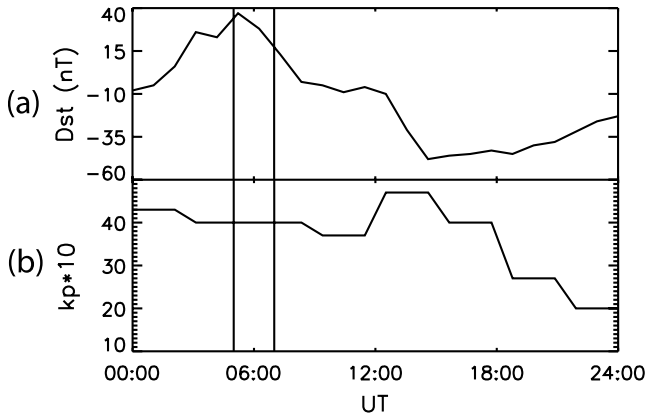


**Figure 2.** (a)  $Dst$  and (b)  $kp*10$  for 11 August 1991. The vertical lines represent the time interval 0500–0700 UT.

where the  $Dst$  index averaged over the event interval was about +27 nT while a sudden storm commencement (SSC) started  $\sim 0250$  UT or about 2 hours prior to the event. The average  $kp$  over the interval was 4 and for the 3 hours prior was 4+, while electron density (not shown) varied slowly from 12 to 17  $e^-/cm^{-3}$  over the interval of 0500–0700 UT. The plasmasphere was compressed with the plasmopause located at  $L \sim 3.9$ . In a previous study of the 11 August 1991 event, *Loto'aniu et al.* [2005] found wave packet ellipticity to be strongly left-hand to linearly polarized.

[13] The EMIC wave event was observed by CRRES with wave packets both below and above the local He+ cyclotron frequency  $f_{He}$ . Table 1 shows the parameters derived from the power spectrograms of the 25 wave packets over the interval 0459–0655 UT. The magnetic field data were converted into field-aligned coordinates,

where the z-component is parallel to the main field direction, the x-component points radially outward and the y-component points eastward completing the right-hand coordinate system.

[14] An event wave packet was defined by the magnetic power spectral density (PSD) maintaining a level above 0.01  $nT^2/Hz$  for at least 60 seconds in either the x-component  $\delta B_x$  or y-component  $\delta B_y$  wavefields. The wavefields were extracted from the total magnetic fields by high pass filtering the magnetic data with a second-order Butterworth filter with a 1-mHz frequency cutoff. The spectral properties of the wave packets in each frequency band were estimated by fitting a three-point normal (Gaussian) distribution to the static wave packet transverse ( $\delta B_x^2 + \delta B_y^2$ ) PSD. The Gaussian fits for two wave packets observed in the interval 0618–0625 UT (Figure 1b) are shown as the dashed lines in Figure 1c. Given the 8 Hz Nyquist for the magnetic data, typical FFT lengths and frequency resolutions for the static spectrograms were 100 s and 0.02 Hz, respectively.

[15] The fitted Gaussian function gives the wave central frequency,  $\omega_m$ , and the wave spectral semibandwidth,  $\delta\omega$ . The total wave magnetic power  $\delta B^2$  was estimated by summing the PSD bins in the range  $\omega_m - \delta\omega$  to  $\omega_m + \delta\omega$  and then multiplying the result by  $\delta\omega$ . The central frequency  $\omega_m/2\pi$  range for all wave packets was 0.29–1.72 Hz, while the full-width half maximum (FWHM)  $\delta\omega/2\pi$  range was 0.06–0.27 Hz. The FWHM  $\delta\omega$  is defined as  $2\sqrt{2 \ln 2} \delta\omega$ .

[16] The  $\delta B^2$  range for the 11 August event was 0.06–6.43  $nT^2$  with an average of 1.59  $nT^2$  for all wave packets. The  $R$  parameter, defined in equation (11) and used in the pitch angle diffusion coefficient equation (8), has a maximum of  $13.6 \times 10^{-5}$  at  $\sim 0531$  UT when  $\delta B^2$  was maximum, while the average  $R$  value is  $3.83 \times 10^{-5}$  for the entire event. Table 1 also shows the local He+ ion cyclotron frequency  $\Omega_{He}$ , and the local plasma density  $N_e$  estimated

**Table 1.** Wave Packet and Local Environment Properties for  $\sim 0459$ –0655 UT on 11 August 1991

Wave Packet	UT	$\omega_m/(2\pi)$ , Hz	$\delta\omega/(2\pi)$ (FWHM), Hz	$\Omega_{He}/(2\pi)$ , Hz	$R(\delta B^2/B_o^2) \times 10^{-5}$	$\delta B^2$ , $nT^2/Hz$	$N_e$ , $e^-/cm^3$
1	4:59:05–5:01:56	1.58	0.20	1.08	1.08	0.85	12
2	5:01:40–5:07:23	1.64	0.19	1.03	8.20	5.95	12
3	5:07:07–5:10:30	1.66	0.14	1.01	0.72	0.50	15
4	5:09:43–5:12:34	1.71	0.14	0.98	0.09	0.06	15
5	5:12:50–5:18:01	1.72	0.21	0.95	2.59	1.60	15
6	5:17:45–5:22:25	1.67	0.27	0.91	0.79	0.45	17
7	5:22:25–5:29:41	1.46	0.16	0.87	8.57	4.43	17
8	5:29:57–5:33:19	1.47	0.20	0.83	13.6	6.43	15
9	5:34:06–5:40:51	1.39	0.12	0.80	7.86	3.42	15
10	5:39:33–5:48:06	1.49	0.15	0.77	10.6	4.27	15
11	5:48:22–5:52:00	1.44	0.20	0.74	1.19	0.45	13
12	5:52:15–5:55:07	1.41	0.21	0.73	5.37	1.93	13
13	6:03:09–6:06:47	1.37	0.27	0.69	2.78	0.89	13
14	6:06:31–6:09:23	1.36	0.19	0.67	2.25	0.69	13
15	6:18:39–6:24:30	1.29	0.22	0.64	7.65	2.11	17
16	6:18:04–6:25:42	0.60	0.06	0.64	7.56	2.07	17
17	6:30:30–6:34:33	0.56	0.08	0.61	0.63	0.16	15
18	6:34:06–6:37:50	0.54	0.09	0.61	0.27	0.07	15
19	6:37:32–6:40:32	0.53	0.12	0.60	3.27	0.80	15
20	6:40:14–6:44:17	0.93	0.13	0.59	1.56	0.37	15
21	6:43:50–6:47:53	0.90	0.12	0.59	3.62	0.85	15
22	6:43:23–6:48:38	0.47	0.11	0.59	1.74	0.41	15
23	6:46:59–6:49:59	0.89	0.11	0.58	0.97	0.22	15
24	6:49:14–6:52:04	0.85	0.08	0.58	0.64	0.15	15
25	6:52:20–6:55:13	0.90	0.12	0.58	2.25	0.51	15

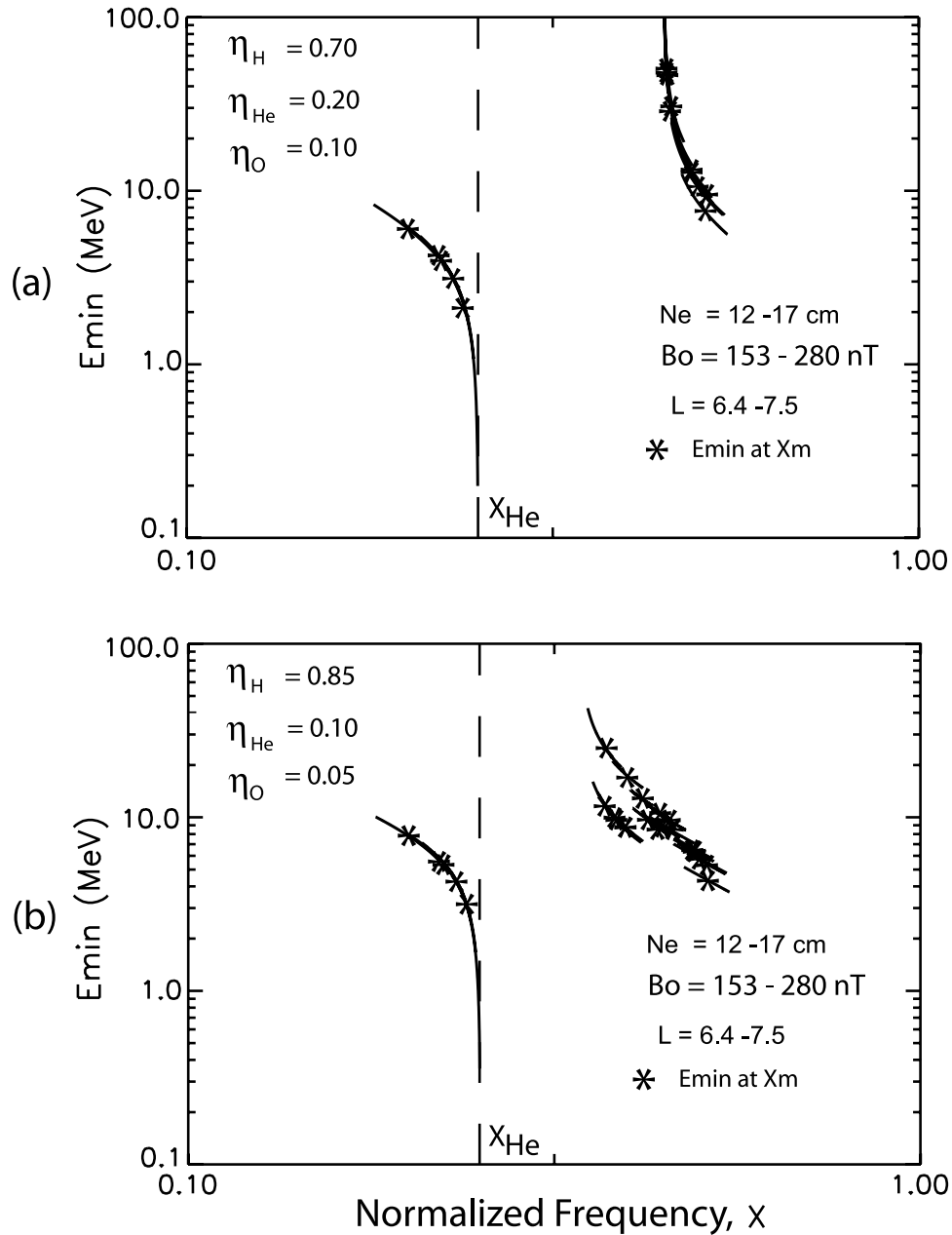


**Figure 3.** Minimum kinetic energy  $E_{\min}$  required by electrons to interact with each of the EMIC wave packets observed by CRRES over the interval  $\sim 0459\text{--}0655$  UT on 11 August 1991 assuming two different ion concentrations of (a)  $\eta_{\text{H}} = 0.70$ ,  $\eta_{\text{He}} = 0.20$ , and  $\eta_{\text{O}} = 0.10$  (stormtime) and (b)  $\eta_{\text{H}} = 0.85$ ,  $\eta_{\text{He}} = 0.10$ , and  $\eta_{\text{O}} = 0.05$  (nominal).

using observations of the upper hybrid resonance frequency  $f_{\text{UHR}}$  [Anderson *et al.*, 1992].

## 5.2. Heavy Ion Concentration

[17] The 11 August event was observed by CRRES in the plasmatrough and during a geomagnetic storm. However, knowledge of the heavy ion composition within the magnetosphere and in particular, the plasmatrough, is difficult owing to the lower plasma density and the high spacecraft charging [Young, 1983]. Furthermore, as pointed out by Meredith *et al.* [2003], there is very little information on the storm dependence of total ion composition in the inner magnetosphere.

[18] Meredith *et al.* [2003] used CRRES data to study the minimum resonant energy  $E_{\min}$  required by electrons to interact with EMIC waves in the magnetosphere. They assumed a stormtime ion composition of 70% H<sup>+</sup>, 20% He<sup>+</sup> and 10% O<sup>+</sup>. Their assumption was based on existing observations suggesting thermal ions dominate the total ion composition in the inner magnetosphere, which for He<sup>+</sup> and O<sup>+</sup> thermal ions are typically 10–20% [Young, 1983; Horwitz, 1987]. Meredith *et al.* repeated their analysis using a lower-percentage heavy ion composition of 85% H<sup>+</sup>, 10% He<sup>+</sup> and 5% O<sup>+</sup>, which they referred to as the nominal ion composition. In this study the  $E_{\min}$  and pitch angle diffusion rate  $D_{\alpha\alpha}$  are both calculated assuming the stormtime

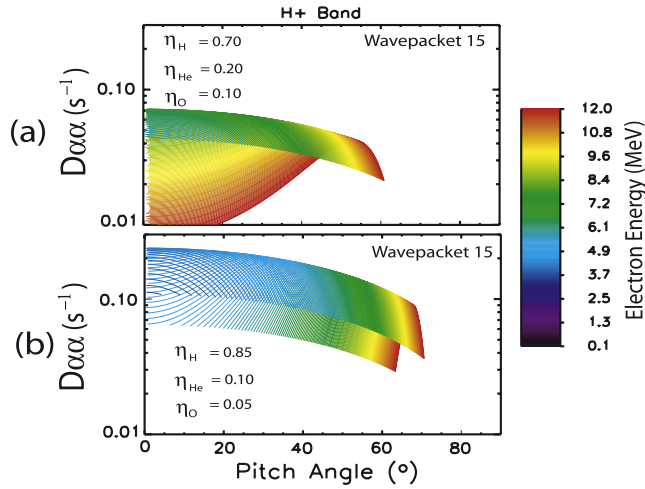


**Figure 4.** H<sup>+</sup> band pitch angle diffusion coefficient  $D_{\alpha\alpha}$  for the event interval  $\sim 0618$ – $0625$  UT (wave packet 15). (a) Assuming a stormtime heavy ion concentration of  $\eta_H = 0.70$ ,  $\eta_{He} = 0.20$ , and  $\eta_O = 0.10$ . (b) Assuming the nominal ion concentration of  $\eta_H = 0.85$ ,  $\eta_{He} = 0.10$ , and  $\eta_O = 0.05$ .

and nominal ion concentrations used by Meredith *et al.* [2003].

### 5.3. Minimum Interaction Energy

[19] Once the wave spectral properties have been determined the minimum energy  $E_m$  over the spectral range defined by  $\omega_1 = \omega - \delta\omega$  to  $\omega_2 = \omega + \delta\omega$  can be calculated using equations (2)–(7). The electron plasma frequency  $\omega_{pe} = (4\pi N_e q_e^2 / m_e)^{1/2}$  in equation (4) can be calculated knowing the local plasma density  $N_e$  and background magnetic field  $B_o$  (section 5.1).

[20] Figure 3a shows the minimum kinetic energy  $E_{\min}$  required by electrons to interact with each of the 25 EMIC wave packets in the interval  $\sim 0459$ – $0655$  UT on 11 August 1991 assuming the stormtime heavy ion ratio of 70% H<sup>+</sup>, 20% He<sup>+</sup> and 10% O<sup>+</sup>, while Figure 3b shows  $E_{\min}$  assuming the nominal ion concentration of 85% H<sup>+</sup>, 10% He<sup>+</sup> and 5% O<sup>+</sup>. In both figures the x-axis is the wave frequency normalized ( $X$ ) to the local H<sup>+</sup> cyclotron frequency while the vertical dashed line in each figure represents the normalized local He<sup>+</sup> cyclotron frequency  $X_{He}$ . The asterisks represent the  $E_{\min}$  values calculated only at the Gaussian fitted normalized central wave frequencies  $X_m$ , while curves represent minimum energies calculated over the full spectral range  $\omega_m - \delta\omega$  to  $\omega_m + \delta\omega$  shown in Table 1.

[21] When only using the central wave frequency to calculate  $E_{\min}$  (asterisks), electrons with energies below

$\sim 2$  MeV do not interact with any of the H<sup>+</sup> or He<sup>+</sup> branch wave packets in both Figures 3a and 3b. In this case, the lowest  $E_{\min}$  is 2.2 MeV associated with wave packet 16 (Table 1) in the He<sup>+</sup> band, assuming stormtime concentrations. Increasing the H<sup>+</sup> ion concentration decreases  $E_{\min}$  in the H<sup>+</sup> band, with lowest minimum energy at  $X_m$  dropping from  $\sim 7.6$  MeV to  $\sim 4.3$  MeV. However, decreasing the He<sup>+</sup> concentration increases the He<sup>+</sup> band  $E_{\min}$  at  $X_m$  with the lowest  $E_{\min}$  increasing from  $\sim 2.2$  MeV to  $\sim 3.1$  MeV. The  $E_{\min}$  were on average higher for the H<sup>+</sup> band wave packets than for the He<sup>+</sup> band wave packets.

[22] Using the full spectral range Gaussian fit properties to calculate  $E_{\min}$ , the minimum energies follow a similar trend to that for the case  $X_m$ . However, there are now ranges of  $E_{\min}$ , with the lowest energy associated with each wave packet falling below the minimum energy at  $X_m$ . As a result, some of the wave packets can interact with  $< \sim 2$  MeV electrons, although they occur only in the He<sup>+</sup> band over the time interval  $\sim 0618$ – $0640$  UT. Table 2 shows a summary of the  $E_{\min}$  results for wave packets in this time interval. During this interval, EMIC wave power was above the selection criteria threshold of  $0.01$  nT<sup>2</sup>/Hz for  $\sim 18$  min. Using the full wave spectral range, relativistic electrons with  $< \sim 2$  MeV could interact with three of the He<sup>+</sup> band wave packets when assuming a stormtime ion concentration. Values for  $E_{\min}$  were lowest for wave packet 16 with electron minimum energy 0.2–3.3 MeV. When the He<sup>+</sup> concentration is decreased to 10% only two wave packets have associated  $E_{\min}$  less than  $\sim 2$  MeV, while wave packet 16 again shows the lowest  $E_{\min}$  of 0.4–4.6 MeV.

### 5.4. Pitch Angle Diffusion Coefficients

[23] The pitch angle diffusion coefficient  $D_{\alpha\alpha}$  can be calculated using equation (8). Values of  $D_{\alpha\alpha}$  as a function of pitch angle  $\alpha$  and electron energy  $E$  were calculated for the five wave packets (see Table 2) observed by CRRES over the interval  $\sim 0618$ – $0640$  UT. The plasma density  $N_e$ ,  $R$  parameter,  $\omega_m$  and  $\delta\omega$  values used in the  $D_{\alpha\alpha}$  calculations are all taken from Table 1.

[24] Figure 4 shows the  $D_{\alpha\alpha}$  for wave packet 15 (H<sup>+</sup> band) using the stormtime and nominal ion concentrations (section 5.2), respectively. In Figure 5, shown is the pitch angle diffusion results for wave packets 16–19 assuming stormtime ion concentration. The results for wave packets 16–19 assuming the nominal ion concentration follows a similar trend to those in Figure 5 and hence are not shown. Note that the energy (color) scale is different between Figures 4 and 5. Also, note that in some of the figures (notably Figure 4), contours fold over as a result of the diffusion rates maximizing at a particular energy and then decreasing afterwards.

**Table 2.** Minimum Electron Energy for the Interval  $\sim 0618$ – $0640$  UT on 11 August 1991

Wave Packet	UT	$\omega_m/(2\pi)$ , Hz	$E_{\min}$ at $\omega_m$ , <sup>a</sup> MeV	$E_{\min}$ Over $\omega_m \pm \delta\omega$ , <sup>a</sup> MeV	$E_{\min}$ at $\omega_m$ , <sup>b</sup> MeV	$E_{\min}$ Over $\omega_m \pm \delta\omega$ , <sup>b</sup> MeV
15	6:18:39–6:24:30	1.29	7.6	5.6–12.5	4.3	3.7–5.1
16	6:18:04–6:25:42	0.60	2.2	0.2–3.3	3.1	0.4–4.6
17	6:30:30–6:34:33	0.56	3.1	1.1–4.6	4.3	1.7–6.1
18	6:34:06–6:37:50	0.54	3.9	2.2–5.5	5.3	3.1–7.1
19	6:37:32–6:40:32	0.53	4.2	1.7–6.5	8.8	2.5–8.0

<sup>a</sup>Based on fixed stormtime ion concentration of  $\eta_H = 0.7$ ,  $\eta_{He} = 0.2$ , and  $\eta_O = 0.1$ .

<sup>b</sup>Based on fixed nominal ion concentration of  $\eta_H = 0.85$ ,  $\eta_{He} = 0.1$ , and  $\eta_O = 0.05$ .

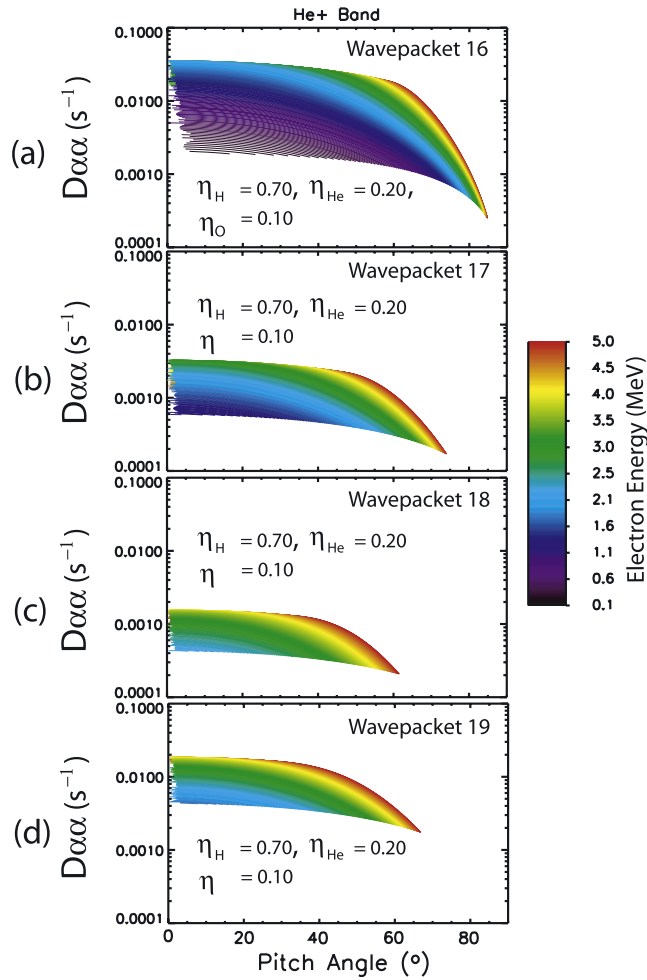


**Figure 5.** He<sup>+</sup> band pitch angle diffusion coefficient  $D_{\alpha\alpha}$  for the 11 August event interval  $\sim 0618$ – $0640$  UT given the stormtime ion concentration of  $\eta_H = 0.70$ ,  $\eta_{He} = 0.20$ , and  $\eta_O = 0.10$ . (a, b, c, d) Results for wave packets 16, 17, 18, and 19, respectively.

[25] Assuming 70% H<sup>+</sup> ions, Figure 4a shows that at higher energies ( $>10$  MeV) the scattering rates for this H<sup>+</sup> band wave packet maximizes at  $D_{\alpha\alpha} \sim 3$ – $4 \times 10^{-2} \text{ s}^{-1}$ , when the pitch angle  $\alpha$  is  $\sim 50$ – $55^\circ$ . The overall scattering rate maximizes at electron energies of 6–8 MeV, where  $D_{\alpha\alpha} \sim 7 \times 10^{-2} \text{ s}^{-1}$  near zero pitch angle. As the energy continues to increase beyond 6–8 MeV the rates start to decrease. In Figure 4b, where the H<sup>+</sup> ion concentration is 85% the pitch angle diffusion rates increase by about a factor of 2 across all energies, when compared to the results in Figure 4a. Here again the fastest rates are close to zero pitch angle for 3–4 MeV electrons where  $D_{\alpha\alpha} \sim 20 \times 10^{-2} \text{ s}^{-1}$ .

[26] In the He<sup>+</sup> band when assuming 20% He<sup>+</sup> ions, the results shown in Figure 5 all follow a similar trend.  $D_{\alpha\alpha}$  generally increases with increasing energies for any given  $\alpha$ , while the rates tend to decrease at fixed energies as  $\alpha$  increases. For wave packet 16 (Figure 5a), the higher energies (3–5 MeV) scattering rates maximize when  $\alpha = 30^\circ$ – $60^\circ$  with  $D_{\alpha\alpha} \sim 2$ – $3 \times 10^{-2} \text{ s}^{-1}$ , while the 1–2 MeV electron scattering rates reach a maximum of  $D_{\alpha\alpha} \sim 1$ – $3 \times 10^{-2} \text{ s}^{-1}$  near  $\alpha = 0^\circ$ . The  $D_{\alpha\alpha}$  results for wave packets 17–

19, shown in Figures 5b–5d, have maximum scattering rates near zero pitch angle when electrons have energies of  $\sim 3$ – $4$  MeV. In these three cases, the fastest scattering rate for  $<2.5$  MeV electrons is  $\sim 10^{-2} \text{ s}^{-1}$  when the electrons are interacting with wave packet 19. The diffusion rates are slowest,  $<10^{-3} \text{ s}^{-1}$ , for  $<2.5$  MeV electrons when scattered by wave packet 18.

[27] As previously mentioned, the pitch angle diffusion results for the He<sup>+</sup> band, in the interval  $\sim 0628$ – $0640$  UT, when using the nominal ion concentration (not shown) follows a similar trend to that when the stormtime concentrations are used. However, the diffusion rates across all energies are in general about two times faster when there are 20% He<sup>+</sup> ions instead of 10%. The  $D_{\alpha\alpha}$  associated with wave packets observed outside the time interval  $\sim 0628$ – $0640$  UT are not shown as the minimum energies related to these wave packets were well above 2 MeV.

## 6. Discussion

[28] The Gaussian-fit central frequency  $\omega_m/2\pi$  range shown in Table 1 is within the usual 0.1–5 Hz EMIC wave frequency observed in the inner magnetosphere [e.g., Fraser and Nguyen, 2001; Loto'aniu et al., 2005]. The  $\delta\omega/2\pi$  FWHM values are  $<\sim 0.3$  Hz for all wave packets, which is consistent with typically quoted EMIC wave bandwidths [e.g., Meredith et al., 2003]. The accuracy of the wave spectral properties is dependent on the accuracy of the normal distribution fits. The greatest error in the curve fitting comes from the lower power range. In this noise region, the power response of instruments which measure quasiperiodic signals often follow a non-Gaussian  $\sim\omega^{-1}$  power distribution. This is the case for the response of the fluxgate magnetometer onboard the CRRES spacecraft [e.g., Loto'aniu et al., 2005]. The inaccuracies due to the instrument natural response were minimized by subtracting signals below 1 mHz before curve fitting. Using the assumption that 90% confidence is required to give reasonable normal distribution fits to the experimental power spectrogram,  $\chi^2$  goodness-of-fit tests (not shown here) showed that all but one wave packet (number 8 in Table 1) lay within this confidence region. Hence the normal distribution fits were good and the assumption that the EMIC wave packet power curve follows a Gaussian shape was reasonable.

[29] The EMIC wave amplitude commonly used in theoretical studies of relativistic electron scattering is 1 nT [Lyons and Thorne, 1972; Summers and Thorne, 2003]. This is consistent with the results shown here where average  $\delta B^2$  for all wave packets is 1.59 nT<sup>2</sup>, corresponding to a root-mean squared (RMS) amplitude of  $\sim 1.3$  nT. However, the  $\delta B^2$  values in Table 1 are likely to be lower limits of the real wave power, since using the standard deviation as the semibandwidth  $\delta\omega$  would underestimate the spectral power. For example, if  $\delta\omega$  is taken as the spectral width where PSD remains above 0.01 nT<sup>2</sup>/Hz, the selection criteria power threshold, average  $\delta B^2$  for all wave packets would be 6.43 nT<sup>2</sup> or 2.5 nT RMS. However, in the derivation of  $D_{\alpha\alpha}$  by Summers and Thorne [2003] the assumption of a normal distribution requires that  $\delta\omega$  represent the standard deviation.

[30] The  $E_{\min}$  results for the 25 wave packets shown in Figures 3a and 3b are consistent with the theoretical study

of *Summers and Thorne* [2003] and the statistical study of *Meredith et al.* [2003], which both found that  $E_{\min}$  depends significantly on the fractional density of the ion that specifies the band and only weakly dependent on the other two fractional ion densities. From the 25 wave packets, the lowest corresponding  $E_{\min}$  values are for wave packets 16–19 (Table 2), which were all observed in the He+ band. These four wave packets occur at central wave frequencies  $\omega_m$  located less than 0.1 Hz from the local He+ cyclotron frequencies  $\Omega_{He}$  (Table 1). The  $\omega_m$  for other wave packets, all observed in the H+ band, were located more than 1 Hz from the local H+ cyclotron frequencies. This result implies that one condition required to lower resonant energies close to the 1–2 MeV range is the presence of EMIC waves at frequencies approaching the ion cyclotron frequency that specifies the wave band [e.g., *Meredith et al.*, 2003; *Summers and Thorne*, 2003].

[31] *Meredith et al.* [2003] calculated  $E_{\min}$  for 416 well-defined polarization EMIC wave events using the central frequency  $\omega_m$  and found  $E_{\min}$  to fall below 2 MeV for  $\sim 11\%$  of the events. The majority of the  $\sim 11\%$  events occurred in the region  $4 < L < 7$ , presumably close to the plasmopause where EMIC wave generation is favorable. They normalized wave frequencies to the equatorial H+ cyclotron frequencies  $\Omega_{Heq}$ . In order to minimize errors associated with assuming a dipole field in mapping  $\Omega_H$  to  $\Omega_{Heq}$ , the 416 events were all observed below  $|MLat| = 25^\circ$ . However, a study by *Hu et al.* [1990] of the integrated wave amplification along the  $L = 6.6$  field-line found that for He+ and H+ band waves, with frequencies in the equatorial stop-band or above, amplification off the equator is significant. Also, a recent study by *Loto'aniu et al.* [2005] suggests a wide EMIC wave generation region up to  $\pm 11^\circ$  off the magnetic equator. The 11 August event was observed well off the equator ( $|MLat| \sim 25^\circ$ ) at  $L \sim 7$  and during stormtime. Given possible off-equator wave generation and the need to assume a field model to determine  $\Omega_{Heq}$ , there is justification in this study for normalizing the wave packet frequencies to the local H+ cyclotron frequencies  $\Omega_H$ . In addition, using realistic wave spectral properties provides a more accurate measure of the minimum energies compared to only using the central wave frequency.

[32] In Table 2, a comparison between the  $E_{\min}$  values calculated using the single frequency  $\omega_m$  and the full spectral width  $2\delta\omega$  clearly demonstrates the importance of using realistic wave spectral properties to estimate minimum interaction energies. For the 11 August event which occurred in the plasmatrough, when using  $\omega_m$  and assuming stormtime ion ratios of  $\eta_H = 0.70$ ,  $\eta_{He} = 0.20$  and  $\eta_O = 0.10$ , Table 2 shows that only 4% (1 wave packet) of the wave packets interact with electrons of energies close to  $\sim 2$  MeV. However, using the spectral width  $2\delta\omega$ , 12–16% (3–4) of the wave packets may interact with electrons of energies  $\sim 2$  MeV or less. Hence using the full wave spectral range on the events studied by *Meredith et al.* [2003] would significantly increase the number of events where  $E_{\min}$  falls below  $\sim 2$  MeV in the region  $4 < L < 7$ . The results here suggest this number may be 3–4 times as many wave packets. This significant increase in the number of EMIC wave packets interacting with the 1–2 MeV electrons may decrease the time taken to scatter electrons into the loss cone. As previously mentioned, the wave packet frequen-

cies in this study were normalized to the local H+ cyclotron frequencies  $\Omega_H$ . However, if the wave generation region was closer to the equator this would reduce the minimum resonant energies and further increase the number of wave packets able to interact with the 1–2 MeV electrons.

[33] The general trend of  $D_{\alpha\alpha}$  in both the H+ and He+ band over the time interval 0618–0640 UT, shown in Figures 4 and 5, agree with the theoretical study of *Summers and Thorne* [2003]. For resonant energies just above the minimum value the scattering rates maximize near the loss cone, while higher energy electrons are scattered more effectively at larger pitch angles. The fastest scattering rates over this time interval were for electrons interacting with the H+ band wave packet 15. Values of  $D_{\alpha\alpha}$  corresponding to the other H+ band wave packets (results not shown) are comparable to the results for wave packet 15, while they all had corresponding  $E_{\min}$  higher than  $\sim 2$  MeV. The 11 August event is typical of the EMIC waves observed in the magnetosphere [e.g., *Fraser and Nguyen*, 2001; *Loto'aniu et al.*, 2005]. The lack of significant flux variability observed during most storms for the much greater than  $>2$  MeV radiation belt electrons could be the result of very fast scattering by EMIC waves.

[34] The overall maximum  $D_{\alpha\alpha}$  for wave packets 15–19 (Table 2) are strongly correlated with the  $R$  parameter (Table 1). For any given ion concentration, the largest  $R$  value are for wave packets 15 and 16, and consequently they also have the fastest diffusion rates out of the five wave packets. These results were expected since  $D_{\alpha\alpha}$  is proportional to  $R$  in the pitch angle diffusion coefficient equation (8). Hence scattering is likely strongest when the background magnetic field strength is low and/or when EMIC waves show strong wave power.

[35] Values of  $D_{\alpha\alpha}$  shown in Figures 4 and 5 have not been averaged over the electron bounce and drift period. Bounce-averaged scattering rates near the loss cone can be an order of magnitude lower [*Lyons and Thorne*, 1972] than the equatorial values given by the quasilinear theory [*Summers and Thorne*, 2003] that is used in this study. It is therefore important to compare the values of  $D_{\alpha\alpha}$  calculated in this study with the strong diffusion rate defined by *Kennel* [1969]. Under strong diffusion, particles diffuse across the loss cone in less than a quarter-bounce period, and the particle flux within the loss cone approaches isotropy [e.g., *Summers and Thorne*, 2003]. The rate at which particles precipitate is then insensitive to the magnitude of the diffusion coefficient.

[36] The mean lifetime or precipitation time  $\tau_{SD}$  for particles under strong pitch angle diffusion has previously been calculated by *Lyons* [1973] and *Schulz* [1974]. Defining  $1/\tau_{SD}$  as the strong pitch angle diffusion coefficient  $D_{SD}$ , *Summers and Thorne* [2003] obtained the following expression for  $D_{SD}$  as a function of  $L$  and electron kinetic energy  $E$ :

$$D_{SD} = \frac{9.66}{L^4} \left[ \frac{4L}{4L-3} \right]^{1/2} \frac{[E(E+2)]^{1/2}}{(E+1)}. \quad (14)$$

Equation (14) was derived assuming a small equatorial loss cone half-angle  $\alpha_o$  approximately equal to  $L^{-3/2}(4-3/L)^{-1/4}$ , a dipole field configuration and particle albedo from the atmosphere  $A = 0.25$ . Figure 6 shows  $D_{SD}$  as a function of  $L$

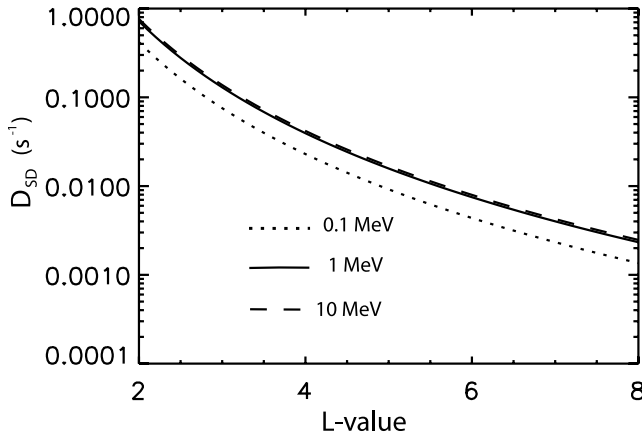


**Figure 6.** Strong pitch angle diffusion coefficient  $D_{SD}$ , as a function of  $L$ , for specified values of electron kinetic energy  $E$  [Summers and Thorne, 2003].

for three values of  $E$ . Note that above  $\sim 1$  MeV the values of  $D_{SD}$  are insensitive to particle energies.

[37] The EMIC wave event was observed when CRRES was located at  $L \sim 7$  where Figure 6 shows  $D_{SD} \sim 4 \times 10^{-3} \text{ s}^{-1}$ . Comparing this value of  $D_{SD}$  to the results in Figure 5, the  $D_{\alpha\alpha}$  associated with wave packets 15, 16 and 19 after bounced-averaging, are likely to be comparable to the strong diffusion limit at  $L \sim 7$  for  $\sim 1$ – $2$  MeV electrons. Hence it is suggested that during the interval  $\sim 0618$ – $0640$  UT on the 11 August 1991  $1$ – $2$  MeV relativistic electrons experienced enhanced scattering due to EMIC wave resonant interactions. This is further suggested since as previously mentioned the use of the standard deviation as the semiband width  $\delta \omega$  likely underestimates the wave power  $\delta B^2$ , which means that values of  $D_{\alpha\alpha}$  shown in Figure 5 are likely to be lower limits.

[38] If the EMIC waves scattered the relativistic ( $>1$  MeV) electrons over the time interval  $\sim 0618$ – $0640$  UT, a decrease in the  $>1$  MeV electron flux levels should be observed around this same time interval by the MEA instrument onboard CRRES. Figure 7a shows the 1-min averaged MEA relativistic flux measurements for the 11 August 1991 over the time interval 0600–0650 UT. The flux values shown were averaged over  $60^\circ$ – $80^\circ$  in pitch angle. As previously mentioned and shown in Figures 4 and 5, pitch angle diffusion rates derived from equation (8), based on quasilinear theory, predicts faster diffusion rates for smaller pitch angles. Unfortunately, owing to the CRRES spacecrafts low-latitude inclination the flux measurements by the MEA instrument are dominated by near-equatorial mirroring (large pitch angle) electrons. During the time interval of the 11 August EMIC wave event reliable MEA relativistic flux measurements were available only for  $\geq 60^\circ$  pitch angle electrons. Nevertheless, as shown in Figure 5, given sufficient EMIC wave power significant pitch angle diffusion rates ( $D_{\alpha\alpha} > 10^{-3} \text{ s}^{-1}$ ) are predicted by quasilinear theory for  $>1$  MeV electrons with  $\sim 60^\circ$ – $80^\circ$  pitch angles. The region in between the vertical dashed lines in Figure 7a represents the time interval  $\sim 0618$ – $0640$  UT.

[39] Figure 7b shows the field-aligned (section 5.1) coordinate (FAC) magnetic field z-component (Bz) for the interval 0600–0650 UT. The solid line is 16-Hz sampled

FAC-Bz, while the dashed line represents FAC-Bz low-pass filtered with a filter cutoff of 1 mHz. CRRES was moving outbound when observing the EMIC wave event and near apogee. This accounts for the overall decreasing trend in flux and the FAC-Bz magnitude over the time interval shown in Figure 7. However, there is an  $\sim 1$  order of magnitude drop in the  $>1$  MeV electron flux levels starting just after  $\sim 0630$  UT and reaching minimum at  $\sim 0640$  UT. The relativistic electron flux levels rise slightly after  $\sim 0640$  UT, coinciding with when the EMIC event wave packets no longer interacted with  $1$ – $2$  MeV electrons. The relativistic flux levels then decreased after  $\sim 0650$  UT (not shown) to below  $\sim 1 \text{ cm}^{-1} \text{ sr}^{-1} \text{ s}^{-1} \text{ MeV}^{-1}$ , or close to the resolvable limit of the MEA instrument. The  $>1$  MeV electron flux levels then remained at this low level as CRRES reached apogee around 0730 UT before flux levels started to increase again around 0920 UT when CRRES was inbound (not shown). The initial flux increase observed during the inbound trip was gradual with the highest energy channel flux level increasing by  $\sim 1$  order of magnitude over about 1 hour.

[40] Low-frequency variations of up to  $\sim 5$ – $10$  nT peak-to-peak amplitudes in the FAC-Bz can be seen in Figure 7b. The field variations are most prominent over the intervals  $\sim 0600$ – $0610$  UT and  $\sim 0630$ – $0650$  UT. However, the  $\sim 1$  order of magnitude flux decrease is limited to the interval  $\sim 0630$ – $0640$  UT. Hence these variations in the field topology were unlikely to be associated with the flux decrease seen during the interval  $\sim 0630$ – $0640$  UT in Figure 7a.

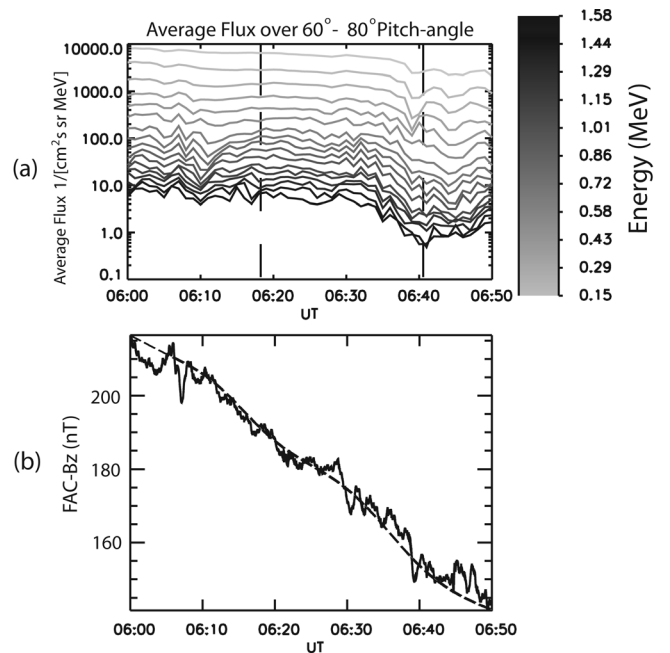


**Figure 7.** (a) CRRES MEA 0.15–1.58 MeV electron flux for the 11 August 1991 over the time interval 0600–0650 UT. The vertical dashed lines represent the time interval when CRRES observed EMIC wave packets which could interact with  $1$ – $2$  MeV electrons. (b) Field-aligned coordinate (FAC) magnetic field z-component (Bz), where the z-axis points along the main field direction.

[41] Relativistic electron flux levels typically fall by several orders of magnitude during the main phase of geomagnetic storms [e.g., Meredith *et al.*, 2002]. This flux decrease is usually attributed to the *Dst* effect [Kim and Chan, 1997; Kim *et al.*, 2002], where relativistic electrons adiabatically respond to decreases in geomagnetic field strength caused by ring current enhancements. The response produces a drop in electron energy, which leads to a drop in flux when measured at a fixed energy. However, as shown in Figure 2 the *Dst* was positive during the EMIC wave event and hence the *Dst* effect can be ruled out as the loss mechanism for relativistic flux decreases seen in Figure 7a at  $\sim 0630$ – $0640$  UT.

[42] Magnetopause shadowing [e.g., Li *et al.*, 1997] may be a possible loss mechanism for the  $> \sim 1$  MeV relativistic electrons over the interval  $\sim 0630$ – $0640$  UT. CRRES was located near apogee at  $L \sim 7$  during the event while the magnetosphere would have been compressed during the initial stage of the geomagnetic storm. It is possible that eastward drifting relativistic electrons on a drift path to intersect CRRES may have been lost to the magnetopause owing to the compression. However, after  $\sim 0640$  UT the relativistic flux levels were observed to rise for about 10 min even though CRRES continued to move toward apogee and hence closer to the magnetopause.

[43] Given the above arguments, it is suggested that the  $\sim 1$  order of magnitude flux decrease in  $> \sim 1$  MeV electrons with  $60^\circ$ – $80^\circ$  pitch angles shown in Figure 7a was the result of pitch angle scattering by EMIC waves over the interval  $\sim 0618$ – $0640$  UT. Since the event occurred during the late stages of a storm initial phase, the results strengthen the suggestion that relativistic electron scattering by EMIC waves can compete with the *Dst* effect as a mechanism of depleting relativistic electron flux levels in the outer zone during initial and main phases of a magnetic storm [e.g., Summers and Thorne, 2003].

[44] Recently, Green *et al.* [2004] studied 52 relativistic electron flux depletion events observed at geostationary orbit. They found that electron flux levels first reduced in the dusk sector concurrent with stretching of the dusk magnetic field to a more tail-like configuration. Their analysis revealed that the flux depletion was likely due to enhanced precipitation into the atmosphere. EMIC waves occur most frequently near geosynchronous in the afternoon sector [e.g., Fraser and McPherron, 1982]. Results presented here suggest that when using realistic spectral wave properties, relativistic flux depletion near geostationary orbit causing enhanced precipitation into the atmosphere can be largely accounted for by scattering of the electrons into the loss cone owing to EMIC wave resonant interaction.

[45] The  $\sim 1$  order of magnitude flux decrease shown in Figure 7a were also observed (not shown here) for  $90^\circ$  pitch angle relativistic electrons. As previously mentioned, the low-latitude inclination of CRRES results in near-equatorial mirroring (large pitch angle) electrons dominating flux observations. The small flux change ( $\sim 1$  order of magnitude) observed over the short time interval of  $\sim 10$  min ( $\sim 0630$ – $0640$  UT) makes it difficult to distinguish flux rates between different pitch angles. Also, the MEA flux data has pitch angle errors of at least 5 degrees. Nevertheless, EMIC wave-particle resonant interaction quasilinear theory cannot explain the scattering of equatorial mirroring

electrons. The question of how  $90^\circ$  pitch angle particles are scattered requires attention, but is beyond the scope of this study. In future studies, it is hoped that this question will be given more attention.

[46] The quasilinear theory used in this study assumes parallel propagation [Summers and Thorne, 2003]. The EMIC waves were observed when CRRES was well off the equator. However, there is justification for using the equatorial quasilinear model of Summers and Thorne [2003] to estimate  $D_{\alpha\alpha}$  in this study. As part of a recent Poynting vector study, Loto'aniu *et al.* [2005] found (although not presented in their paper) that during the interval  $\sim 0615$ – $0710$  UT on 11 August, the angle between the field-aligned EMIC wave Poynting vector and the background magnetic field was less than  $30^\circ$ . Also, a recent theoretical study by Albert [2003] showed that pitch angle diffusion coefficients for waves propagating at  $25^\circ$  to the equator were quite similar to the on-equatorial results of Summers and Thorne [2003]. Furthermore, this study is the first time that realistic EMIC wave packet spectral properties have been applied to any model of relativistic electron pitch angle scattering in the magnetosphere.

## 7. Conclusions

[47] Knowledge of the EMIC wave spectral properties is required in order to understand the relative importance of resonant scattering of 1–2 MeV electrons in the magnetosphere. Previous observational studies have calculated minimum energy  $E_{\min}$  using a single frequency to represent the EMIC wave packet. The results in this study show that when  $E_{\min}$  is estimated based on more realistic spectral properties the number of wave packets able to interact with 1–2 MeV electrons in the outer radiation belt may significantly increase.

[48] The 11 August event occurred when a geomagnetic storm was entering its main phase. Decreases in relativistic flux levels often observed during storm main phase are usually attributed to the well-known *Dst* effect. However, the results presented here suggest that nonadiabatic scattering by EMIC waves is a significant contributor to relativistic electron losses during the initial and main phase of storms. The conclusions from this research are based on one long duration event consisting of 25 wave packets. It is hoped that a future paper based on the statistical results from over 200 EMIC wave packet events, which were initially studied by Loto'aniu *et al.* [2005], will provide further definitive conclusions on the importance of resonant scattering of 1–2 MeV electrons due to EMIC waves during geomagnetic storms.

[49] **Acknowledgments.** This work was supported by NASA grant NNG04GN44G. D. S. acknowledges support from the Natural Sciences and Engineering Research Council of Canada under grant A-0621. T. M. L. and B. J. F. thank R. A. Anderson for providing the CRRES electron density data and H. J. Singer for providing the AFGL magnetometer data. We thank both of the reviewers for their comments and suggested changes.

[50] Lou-Chuang Lee thanks Nigel Meredith and the other reviewer for their assistance in evaluating this paper.

## References

Albert, J. M. (2003), Evaluation of quasi-linear diffusion coefficients for emic waves in a multispecies plasma, *J. Geophys. Res.*, *108*(A6), 1249, doi:10.1029/2002JA009792.

- Anderson, R. R., D. Gurnett, and D. Odem (1992), CRRES plasma wave experiment, *J. Spacecr. Rockets*, *29*, 570–573.
- Baker, D. N., J. B. Blake, L. B. Callis, J. R. Cummings, D. Hovestadt, S. Kanekal, B. Klecker, R. A. Mewaldt, and R. D. Zwickl (1994), Relativistic electron acceleration and decay timescales in the inner and outer radiation belts: Sampex, *Geophys. Res. Lett.*, *21*, 409–412.
- Blake, J. B., W. A. Kolasinski, R. W. Filius, and E. G. Mullen (1992), Injection of electrons and protons with energies of tens of MeV into 1–3 on March 24, 1992, *Geophys. Res. Lett.*, *19*, 821–824.
- Bräysy, T., K. Mursula, and G. Marklund (1998), Ion cyclotron waves during a great magnetic storm observed by Freja double-probe electric field instrument, *J. Geophys. Res.*, *103*, 4145–4155.
- Elkington, S. R., M. K. Hudson, and A. A. Chan (1999), Acceleration of relativistic electrons via drift-resonance interactions with toroidal-mode Pc 5 ULF oscillations, *Geophys. Res. Lett.*, *26*, 3273–3276.
- Elkington, S. R., M. K. Hudson, and A. A. Chan (2003), Resonant acceleration and diffusion of outer zone electrons in an asymmetric geomagnetic field, *J. Geophys. Res.*, *108*(A3), 1116, doi:10.1029/2001JA009202.
- Erlanson, R., and A. J. Ukhorskiy (2001), Observations of electromagnetic ion cyclotron waves during geomagnetic storms: Wave occurrence and pitch-angle scattering, *J. Geophys. Res.*, *106*, 3883–3895.
- Foat, J. E., et al. (1998), First detection of a terrestrial MeV X-ray burst, *Geophys. Res. Lett.*, *25*, 4109–4112.
- Fraser, B., and R. McPherron (1982), Pc 1-2 magnetic pulsation spectra and heavy ion effects at synchronous orbit: Ats 6 results, *J. Geophys. Res.*, *87*, 4560–4566.
- Fraser, B. J., and T. S. Nguyen (2001), Is the plasmopause a preferred source region of electromagnetic ion cyclotron waves in the magnetosphere?, *J. Atmos. Sol. Terr. Phys.*, *63*, 1225–1247.
- Fraser, B., H. Singer, W. Hughes, J. Wygant, R. Anderson, and Y. Hu (1996), CRRES Poynting vector observations of electromagnetic ion cyclotron waves near the plasmopause, *J. Geophys. Res.*, *101*, 15,331–15,343.
- Friedel, R. H. W., G. D. Reeves, and T. Obara (2002), Relativistic electron dynamics in the inner magnetosphere—A review, *J. Atmos. Sol. Terr. Phys.*, *64*, 265–282.
- Fung, S. F. (2004), Survey of current situation in radiation belt modeling, *Adv. Space Res.*, *34*, 1441–1450.
- Green, J. C., T. G. Onsager, T. P. O'Brien, and D. N. Baker (2004), Testing loss mechanisms capable of rapidly depleting relativistic electron flux in the Earth's outer radiation belt, *J. Geophys. Res.*, *109*, A12211, doi:10.1029/2004JA010579.
- Home, R. B., and R. M. Thorne (1998), Potential waves for relativistic electron scattering and stochastic acceleration during magnetic storms, *Geophys. Res. Lett.*, *25*, 3011–3014.
- Horwitz, J. L. (1987), Core plasma in the magnetosphere, *Rev. Geophys.*, *25*, 579–587.
- Hu, Y. D., B. J. Fraser, and J. V. Olson (1990), Amplification of electromagnetic ion cyclotron waves along wave paths in the Earth's multi-component magnetosphere, *Geophys. Res. Lett.*, *17*, 1053–1056.
- Johnson, M. H., and J. K. Ball (1992), Combined release and radiation effects satellite (CRRES): Spacecraft and mission, *J. Spacecr. Rockets*, *29*, 556–563.
- Kennel, C. (1969), Consequences of a magnetospheric plasma, *Rev. Geophys.*, *7*, 379–419.
- Kim, H.-J., and A. A. Chan (1997), Fully adiabatic changes in storm time relativistic electron fluxes, *J. Geophys. Res.*, *102*, 22,107–22,116.
- Kim, H.-J., G. Rostoker, and Y. Kamide (2002), Radial dependence of relativistic electron fluxes for storm main phase development, *J. Geophys. Res.*, *107*(A11), 1378, doi:10.1029/2001JA007513.
- Li, X., et al. (1997), Multisatellite observations of the outer zone electron variation during the November 3–4, 1993, magnetic storm, *J. Geophys. Res.*, *102*, 14,123–14,140.
- Lorentzen, K. R., M. P. McCarthy, G. K. Parks, J. E. Foat, R. M. Millan, D. M. Smith, R. P. Lin, and J. P. Treilhou (2000), Precipitation of relativistic electrons by interaction with electromagnetic ion cyclotron wave, *J. Geophys. Res.*, *105*, 5381–5390.
- Loto'aniu, T. M., B. J. Fraser, and C. L. Waters (2005), The propagation of electromagnetic ion cyclotron wave energy in the magnetosphere, *J. Geophys. Res.*, *110*, A07214, doi:10.1029/2004JA010816.
- Lyons, L. (1973), Comments on pitch angle diffusion in the radiation belts, *J. Geophys. Res.*, *78*, 6793–6797.
- Lyons, L. R., and R. M. Thorne (1972), Parasitic pitch angle diffusion of radiation belt particles by ions cyclotron waves, *J. Geophys. Res.*, *77*, 5608–5616.
- Mathie, R. A., and I. R. Mann (2000), A correlation between intervals of ULF wave power and storm-time geosynchronous relativistic electron flux enhancements, *Geophys. Res. Lett.*, *27*, 3261–3264.
- Mathie, R. A., and I. R. Mann (2001), On the solar wind control of PC5 ULF pulsation power at mid-latitudes: Implications for MeV electron acceleration in the outer radiation belt, *J. Geophys. Res.*, *106*, 29,783–29,796.
- Meredith, N. P., R. B. Horne, D. Summers, R. M. Thorne, R. H. A. Iles, and D. Heynderickx (2002), Evidence for acceleration of outer zone electrons to relativistic energies by whistler mode chorus, *Ann. Geophys.*, *20*, 967–979.
- Meredith, N. P., R. M. Thorne, R. B. Horne, D. Summers, B. J. Fraser, and R. R. Anderson (2003), Statistical analysis of relativistic electron energies for cyclotron resonance with emic waves observed on CRRES, *J. Geophys. Res.*, *108*(A6), 1250, doi:10.1029/2002JA009700.
- Millan, R. H. (2002), X-ray observations of MeV electron precipitation with a balloon-borne germanium spectrometer, Ph.D. thesis, Dep. of Phys., Univ. of Calif., Berkeley.
- O'Brien, T. P., K. R. McPherron, I. R. Mann, N. P. Meredith, J. B. Blake, J. F. Fennell, M. D. Looper, D. K. Milling, and R. R. Anderson (2003), Energization of relativistic electron in the response of ULF power and MeV microbursts: Evidence for dual ULF and VLF acceleration, *J. Geophys. Res.*, *108*(A8), 1329, doi:10.1029/2002JA009784.
- Reeves, G. D., K. L. McAdams, R. H. W. Friedel, and T. P. O'Brien (2003), Acceleration and loss of relativistic electrons during geomagnetic storms, *Geophys. Res. Lett.*, *30*(10), 1529, doi:10.1029/2002GL016513.
- Rostoker, G., S. Skone, and D. N. Baker (1998), On the origin of relativistic electrons in the magnetosphere associated with some geomagnetic storms, *Geophys. Res. Lett.*, *25*, 3701–3704.
- Schulz, M. (1974), Particle lifetimes in strong diffusion, *Astrophys. Space Sci.*, *31*, 37–42.
- Singer, H. J., W. P. Sullivan, P. Anderson, F. Mozer, P. Harvey, J. Wygant, and W. McNeil (1992), Fluxgate magnetometer instrument on the CRRES, *J. Spacecr. Rockets*, *29*, 599–601.
- Steinacker, J., and J. A. Miller (1992), Stochastic electron acceleration in a low-beta plasma: I. Interaction with parallel transverse cold plasma waves, *Astrophys. J.*, *393*, 764–781.
- Summers, D., and R. H. Thorne (2003), Relativistic electron pitch-angle scattering by electromagnetic ion cyclotron wave during geomagnetic storms, *J. Geophys. Res.*, *108*(A4), 1143, doi:10.1029/2002JA009489.
- Summers, D., R. H. Thorne, and F. Xiao (1998), Relativistic theory of wave-particle resonant diffusion with application to electron acceleration in the magnetosphere, *J. Geophys. Res.*, *103*, 20,487–20,500.
- Summers, D., C. Ma, and T. Mukai (2004), Competition between acceleration and loss mechanisms of relativistic electrons during geomagnetic storms, *J. Geophys. Res.*, *109*, A04221, doi:10.1029/2004JA010437.
- Thorne, R. H., and L. J. Andreoli (1980), Mechanisms for intense relativistic electron precipitation, in *Exploration of the Upper Atmosphere*, edited by D. Deehr and J. A. Holtet, pp. 381–394, Springer, New York.
- Thorne, R. H., and C. F. Kennel (1971), Relativistic electron precipitation during magnetic storms main phase, *J. Geophys. Res.*, *76*, 4446–4453.
- Thorne, R. H., R. B. Horne, S. A. Glauert, N. P. Meredith, Y. Y. Shprits, D. Summers, and R. R. Anderson (2005), The influence of wave-particle interactions on relativistic electron dynamics during storms, in *Inner Magnetosphere Interactions: New Perspectives From Imaging*, *Geophys. Monogr. Ser.*, vol. 159, edited by J. Burch, M. Schulz, and M. Spence, pp. 101–112, AGU, Washington, D. C.
- Young, D. T. (1983), Heavy ion plasmas in the outer magnetosphere, *J. Geophys. Res.*, *88*, 167–175.

B. J. Fraser, Cooperative Research Centre for Satellite Systems, School of Mathematical and Physical Sciences, University of Newcastle, Newcastle, NSW 2308, Australia. (bjf@newcastle.edu.au)

T. M. Loto'aniu, Department of Physics, University of Alberta, Edmonton, Alberta, T6G 2J1, Canada. (lotoaniu@phys.ualberta.ca)

D. Summers, Department of Mathematics and Statistics, Memorial University of Newfoundland, St. John's, NL A1C 5S7, Canada. (dsummers@math.mun.ca)

R. M. Thorne, Department of Atmospheric Sciences, University of California, Los Angeles, Los Angeles, CA 90095-1565, USA. (rmt@atmos.ucla.edu)